Toward Consistent Regional-to-Global-Scale Vegetation Characterization Using Orbital SAR Systems

Josef M. Kellndorfer, Leland E. Pierce, *Member, IEEE*,
M. Craig Dobson, *Senior Member, IEEE*, and Fawwaz T. Ulaby, *Fellow, IEEE*

***Abstract*— A study was conducted to assess the potential of combined imagery from the existing European and Japanese orbital synthetic aperture radar (SAR) systems, ERS-1 (C-band, VV-polarization) and JERS-1 (L-band, HH-polarization), for regional-to-global-scale vegetation classification. For seven test sites from various ecoregions in North and South America, ERS-1/JERS-1 composites were generated using high-resolution digital elevation model (DEM) data for terrain correction of geometric and radiometric distortions. An edge-preserving speckle reduction process was applied to reduce the fading variance and prepare the data for an unsupervised clustering of the two-dimensional (2-D) SAR feature space. Signature-based classification of the clusters was performed for all test sites with the same set of radar backscatter signatures, which were measured from well-defined polygons throughout all test sites. While trained on one-half of the polygons, the classification result was tested against the other half of the total sample population. The multisite study was followed by a multitemporal study in one test site, clearly showing the necessity of including multitemporal data beyond a level 1 (woody, herbaceous, mixed) vegetation characterization. Finally, classifications with simulation of backscatter variations shows the dependence of the classification results on calibration accuracy and on naturally occurring backscatter changes of natural surfaces. Overall, it is demonstrated that the combination of existing orbital L- and C-band SAR data is quite powerful for structural vegetation characterization.**

***Index Terms*— Classification image, ERS-1, JERS-1, synthetic aperture radar (SAR), vegetation mapping.**

I. Introduction

DECADES of research in various geoscientific disciplines concerned with the impacts of global (climate) change led to the formulation of biogeophysical models to describe global cycles, e.g., of water and carbon. Significant understanding of many processes and variables emerged from research within the framework of the *International Geosphere and Biosphere Program* (IGBP), which was launched in 1986 by the International Council of Scientific Unions (ICSU). Research results from IGBP and related programs [World Climate Research Program (WCRP) and International Human Dimensions Program (IHDP)] led to the postulation of *global observing systems*, which should provide accurate data to validate, refine, and run the models. After the definition of plans for the *Global Ocean Observation System* (GOOS) and *Global Climate Observation System* (GCOS), the *Global Terrestrial Observation System* (GTOS) was established by Food and Agriculture Organization (FAO), United Nations Environment Program (UNEP), United Nations Educational, Scientific, and Cultural Organization (UNESCO), World Meteorological Organization (WMO), and ICSU in January 1996. A joint *Terrestrial Observation Panel for Climate* (TOPC) of GTOS and GCOS released a plan for *terrestrial climate-related observations* in June 1997 [1]. The objective of this plan is to provide a rationale for the structure and implementation for an initial observing system (IOS). The TOPC formulated in a very detailed fashion the status and observational requirements for a minimum set of variables grouped in biophysical properties of vegetation, land use/cover and disturbance, soil properties, radiation, hydrology, biochemistry, cryospheric properties, and trace gases. While some variable measurements can only be carried out *in situ* (e.g., soil nutrient content), the TOPC expresses high hopes in the use of remote-sensing systems and encourages research to assess existing and planned systems for their global observation potential.

With the launch of orbital radar imaging satellites in the 1990's, a new era in remote sensing began. After the successful, but short, lifetime mission of Seasat in 1978 and several shuttle imaging radar (SIR) missions, geoscientific earth observation with satellites operating in the visible and near-infrared portions of the electromagnetic spectrum, is now complemented by radar systems that provide global, multitemporal, multifrequency, and multipolarization synthetic aperture radar (SAR) imagery at spatial (order < 100 m) and temporal (order one month) high resolution. While the

TABLE I
SENSOR CHARACTERISTICS

Satellite	ERS-1	JERS-1
Launched by	ESA, Europe	NASDA, Japan
in	July 1991	April 1992
Frequency	C-Band, 5.3 Ghz	L-Band,1.25Ghz
Wavelength	5.6 cm	23 cm
Polarization	VV	HH
Resolution	30m	18m
Incidence Angle	23o	35o
Swath width	100km	75km
Orbit	polar	polar

Manuscript received November 17, 1997; revised April 27, 1998.

The authors are with the Radiation Laboratory, The University of Michigan, Ann Arbor, MI 48109-2122 USA (e-mail: josefk@eecs.umich.edu).

Publisher Item Identifier S 0196-2892(98)06837-5.

TABLE II
REQUIREMENTS FOR THE GLOBAL OBSERVATION OF SELECTED VARIABLES, AS DEFINED IN [1]

Variable	Units of measurements	Temporal resolution	Spatial resolution	Accuracy
Biomass, above ground	g/m^2	Once every 5 years	100 m – 1000 m	10%
Leaf area index (LAI)	m^2/m^2	10 – 30 days	250 m – 1000 m	5–10%
Roughness (surface)	m	5 years	1–10m at 1–10km intervals	±10%
Spectral vegetation greenness index	dimensionless	10 – 30 days	250 m – 1000 m	0.02 at a range from -1 to +1
Vegetation structure	Qualitative classes of structure (non-woody annuals and perennials; shrub land, savanna, open forest, closed forest); also as a continuous variable measured in mT/ha	1 year to 10 years	30 m – 1000 m	± 10%
Fire area	km^2	30 days	1 km	10%
Land cover	Land cover class	1 year to 5 years	0.25–0.5 km for global, 30 m for regional to local	80% for operation of GCMs; 95%, e.g., for estimating changes in carbon stocks and detecting cover boundaries
Land use	Land use class	5 years	5 m – 1 km depending on the spatial heterogeneity of land use; at least 30 m for many regions	TBD

now-orbiting remote-sensing satellites, ERS-1/2, JERS-1, and Radarsat, carry all single-frequency and single-polarization SAR instruments, the new generation of planned SAR systems will provide multipolarization (e.g., LightSAR, PALSAR, and Envisat) and possibly multifrequency/multipolarization data (e.g., LightSAR).

The close physical relationship of SAR backscatter measurements and vegetation structural attributes has been pointed out by many authors [2]–[4]. After theoretical results from simulations of SAR backscatter of vegetation in C_{vv} and L_{hh} and encouraged by first preliminary results on the use of combined ERS-1/JERS-1 (Table I) data for structural land-cover characterization, a more thorough study was conducted at The University of Michigan, Ann Arbor, over the past years. Led by the needs of the global change research community, as now expressed in clearly defined requirements for vegetation observation (Table II) by the TOPC, the potential of ERS-1/JERS-1 SAR data for regional-to-global-scale vegetation characterization was investigated. The study focused (so far) on the testing of a radar classifier based on the assumption that structurally and electrically similar vegetation, no matter where it appears on earth, has similar backscattering behavior. Furthermore, since radar is an active sensing system with constant illumination geometry and well-known transmit/receive power spectra, radar imagery can be calibrated to a very high degree of accuracy, thus allowing the comparison of backscatter values (σ°) over time and space.

The project was designed to acquire ERS-1/JERS-1 scenes from locations in different ecoregions, apply identical preprocessing procedures for radiometric and geometric correction of the imagery, and develop and test a single classification protocol for all scenes. Even if limited to one frequency and polarization, it is the potential of orbital SAR systems to guarantee multitemporal "cloud-free" data sets, which provides significant advantages over optical systems. Although no multisite/multitemporal data sets were available to us at this point, we were able to conduct a study on the classification results using multitemporal data from the test site Raco, MI.

Fig. 1. Location of the test sites in various ecoregions. Cabaliana and Raco were super sites for the SIR-C/X-SAR campaigns in April and October 1994. All other sites are LTER sites.

The main aim of this paper is to present the results of this study to the science user community to support assessment of the potential and limitations of existing orbital SAR systems ERS-1 and JERS-1 for vegetation mapping purposes at regional-to-global scales. In addition, the classification methodology described here is suggested to provide a simple, hence widely applicable, approach for use with large-scale SAR data sets.

II. TEST SITES

Fig. 1 shows the location of the test sites where radar images from both ERS-1 and JERS-1 have been used to measure backscattering values from vegetation. The test sites were selected to get a representative cross section through various biomes and to optimize access to available ground-truth (polygons) data. Two of the test sites reported here were super sites (Raco and Cabaliana, Brazil) for the SIR campaign in 1994 (SIR-C/X-SAR), and five test sites are part of the

National Science Foundation (NSF) network of long-term ecological research sites (LTER). These sites are operated to conduct long-term research, and hence good knowledge of the localities is given. Invaluable support through and cooperation with local site scientists made it possible to acquire necessary ground truth for image interpretation and analysis.

Raco (46°25′N 85°00′W) is a test site managed by the Radiation Laboratory, The University of Michigan. Eighty forest stands and many pasture and wetland areas have been biometrically surveyed over the course of five years, and extensive ground truth is available. All forest test plots are at least 4 ha in size. They encompass mainly pines (jack pine, red pine, and white pine) and northern hardwoods (sugar maple, red maple, aspen, and beech) at different growth stages.

Kellogg, MI, (42°28′N 85°27′W) is a forested site under investigation by the Kellogg Biological Station. The forest composition is similar to the Raco test site with scattered stands of pines, oak-hickory, and beech-maple deciduous midlatitude forest, wetlands, and agriculture.

Cedar Creek, MN, (45°24′N 93°12′W) Natural History Area is operated by the University of Minnesota, Minneapolis, in cooperation with the Minnesota Academy of Sciences. It lies at the boundary between prairie and midlatitude forest and is a mosaic of uplands dominated by oak savannah, prairie, hardwood forest, pine forest, and abandoned agricultural fields and of lowlands comprising oak and cedar swamps, acid bogs, marshes and sedge meadows.

Konza Prairie, KS, (39°05′N 96°35′W) is managed by Kansas State University, Manhattan, to provide an array of burning and grazing treatments (mainly buffalo) to facilitate ecological research. Lowland areas have patches of native prairie grass species, especially big bluestem, indian grass, little bluestem, and switchgrass that grow to 2–3 m during the summer. Some gallery forests are dominated by bur and chinguapin oaks with green ash, hackberry, elm, and black walnut.

The **Sevilleta Wildlife Refuge, NM,** (34°18′N, 106°48′W) is located at multiple intersections of subalpine mixed-conifer forest/meadow, riparian cottonwood forest, dry mountain land, grassland, cold desert, and hot desert. The main communities found are conifer savannah, creosote bush, desert grassland, mesquite and sand dunes, Great Basin shrub and shortgrass steppes, and tallgrass swales and riparian.

The **Jornada Experimental Range, NM,** (32°30′N, 106°45′W) research conducted by the New Mexico State University, Las Cruces, focuses on five habitat types: black gamma grassland, creosote bush scrub, mesquite duneland, tarbush shrublands, and playa. The playas are dominated by a variety of grasses and found in low-lying, periodically flooded areas.

The **Cabaliana** (3°18′S 60°59′W) test site has been investigated by the University of California, Santa Barbara, for the SIR-C/X-SAR campaign. The study area includes a wide variety of vegetation typical of wetlands in the central Amazon basin. The annual rise of the Solimoes River inundates large forested areas of the floodplain (varçea). Other wetland types within the study area include shrublands and very open woodlands occurring in low-lying areas, with clumps of trees or shrubs interspersed with open water and aquatic macrophyte beds. Upland forests (terra firme) and clearcuts with second growth are found in this test site as well [6].

TABLE III
SAR SENSITIVITY TO A HIERARCHICAL VEGETATION CLASSIFICATION SCHEME BASED ON PLANT PHYSIOGNOMY, AS PROPOSED BY THE UNITED STATES FEDERAL GEOGRAPHIC DATA COMMITTEE [7]. IN EACH HIERARCHICAL LEVEL, NEW PHYSIOGNOMIC MODIFIERS ARE INTRODUCED. ADDITIONAL MODIFIERS (E.G., CLIMATE, NATURAL/PLANTED) EXIST, HOWEVER, WITHOUT A DIRECT LINK TO SAR SENSITIVITY. ADDITIONAL GEOGRAPHIC KNOWLEDGE FOR LOCAL ADAPATION OF SAR-DERIVED VEGETATION MAPS IS NECESSARY

FGDC Proposed Standard	SAR Sensitivity
Physiognomic class:	
Peak % cover in Upper Strata, Average Vegetation Height	
Closed Tree Canopy	(Woody) Biomass
Open Tree Canopy	Macro-Structure of
Shrubland	Vegetation
Dwarf Shrubland	"Main/Small Stems"
Herbaceous	
Non-Vascular	
Physiognomic Subclass	
Leaf phenology	
Evergreen (e.g. *Tree Canopy*)	Multitemporal Observations
Perennial (e.g. *Herbaceous*)	
Deciduous (e.g. *Tree Canopy*)	
Annual (e.g. *Herbaceous*)	
Physiognomic Group	
Leaf Morphology, Climate	
e.g *Closed Tree Canopy:*	
Broadleaf	(Woody) Biomass
Needleaf	Micro-Structure of
e.g. *Herbaceous* (Temparate Climate)	Vegetation
Plain Grassland	"Foliage"
with a Tree Layer	
with a Shrub Layer	
with a Dwarf Shrub Layer	
Formation	
e.g. *Hydrological modifiers*	
Dry Conditions	"(Soil) Moisture"
Wet Conditions	

III. SCENE SELECTION

Besides the availability of JERS-1 scenes for the test sites, three major criteria were considered when selecting scenes for the study.

1) Seasonality: To keep the structural appearance of vegetation comparable (e.g., deciduous trees are not defoliated), it was decided to select scenes during the peak of the phenological year. Selecting the peak of the vegetation period also conforms with the *proposed standard for vegetation classification* [7]. This vegetation classification scheme was used as a protocol to communicate polygon labels between the ERS-1/JERS-1 project group and the collaborators in the test sites. Also, the hierarchical approach based on plant physiognomy relates to SAR measurements very closely (Table III) [8]. In the multitemporal study, scenes of the "phenological growing hiatus" were selected since especially frozen, leaf off, and postharvest conditions (with tilled ground) are clearly detectable changes in the radar signal [9], [10].

2) Moisture Conditions: Radar is sensitive to moisture changes in soil and canopy, and hence, wet conditions significantly alter backscattering values that will lead to a certain decrease in classification accuracy when moist and dry scenes are classified under the same rules. A careful selection of scenes from relatively dry periods (no rain on,

TABLE IV
TEST SITE LOCATIONS, ERS-1/JERS-1 ACQUISITION DATES, AND PRECIPITATION HISTORY FOR ACQUISITION DATES

Test Site	Latitude	Longitude	ERS-1 Date	ERS-1 Time GMT/Local	ERS-1 Precipitation on acquisition date [mm]	ERS-1 Precipitation history 5 days (d) prior to datatake (DT)	JERS-1 Date	JERS-1 Time GMT/Local	JERS-1 Precipitation on acquisition date [mm]	JERS-1 Precipitation history 5 days (d) prior to datatake (DT)	Days difference between datatakes
Raco Hiawatha National Forest	46°25'N	85°00'W	17-AUG-92	16:30/11:30	0	0 mm	07-AUG-92	16:25/11:25	0	1 mm 5 d before DT	10
			3-FEB-93	16:30/11:30	0	0 mm	21-OCT-93	16:24/11:24	16	20 mm 5 d before DT, 2 mm 2 d before DT	10
Kellogg Biological Station (Lux Arbor)	42°28'N	85°27'W	29-JUL-92	16:28/11:28	0	sum of 6 mm up to 3 d before DT	07-AUG-92	16:26/11:26	0	0 mm	8
Cedar Creek Natural History Area	45°24'N	93°12'W	10-SEP-94	17:03/11:03	2	sum of 3 mm up to 4 d before DT	09-SEP-94	16:56/10:56	2	2 mm 5 d before DT	1
Konza Prairie Research Natural Area	39°05'N	96°35'W	25-JUN-94	17:09/11:09	0	sum of 33 mm on days 3 and 4 before DT	31-JUL-94	17:06/11:06	0	0 mm	36
Sevilleta National Wildlife Refuge	34°18'N	106°48'W	28-APR-94	17:47/10:47	0	0 mm	6-APR-94	17:42/10:42	0	0 mm	22
Jornada Basin	32°30'N	106°45'W	18-MAY-94	17:45/10:45	0	0 mm	6-APR-94	17:42/10:42	0	0 mm	42
Cabaliana, Amazon Basin	3°18'S	60°59'W	06-OCT-93	14:20/10:20	NA	low water season, daily precipitation assumed	03-OCT-93	14:22/10:22	NA	low water season, daily precipitation assumed	3

and a couple of days before, the image acquisition) helped to minimize shifts in the signal due to soil moisture changes and intercepted rain on the vegetation canopy and stems. However, wet ground/vegetation conditions are predominant in many regions, e.g., the tropics, which might lead to the necessity to apply a moisture-adjusted set of classification rules.

3) Scene Overlap: Naturally, with a multisensoral study, the overlap of scenes is a key issue and this selection criteria is twofold: time and space. During scene selection, combinations were preferred that 1) maximized the area covered by both sensors and minimized the time span between the two acquisition dates of the same phenological stages.

While this study used composites of single ERS-1 and JERS-1 scenes, large regional mosaics of forested tropical regions of the earth are currently produced in the framework of programs like TREES and *Global Rain Forest Mapping* (GRFM) [11]. The *Global Boreal Forest Mapping* (GBFM) with ERS-1 and JERS-1 SAR is planned after an existing gap in ERS-1 SAR coverage of Siberia has been closed with the deployment of the German mobile ERS-1 receiving station in Ulan Bator, Mongolia [12].

For the seven test sites, it was possible to select scenes with good overlap, satisfying precipitation history, and acquisition date differences ranging from one to 42 days (Table IV).

IV. GENERATION OF THE ERS-1/JERS-1 COMPOSITES

To generate absolutely calibrated ERS/JERS-1 SAR image composites, a preprocessing chain was designed and implemented at the Microwave Image Processing Laboratory, The University of Michigan. To perform orthorectification, radiometric calibration, and the generation of the value-added products (layover/shadow masks, local incidence angle map), software was developed at The University of Michigan in cooperation with the Vexcel Corporation, Boulder, CO. The orthorectification part of the software is based on the algorithms published in [13] and [14]. The calculation of the local incidence angle follows [15]. The developed method for the determination of layover and shadow is described in [16]. Fig. 2 gives an overview over the input and output products of the geocoding process.

TABLE V
CHARACTERISTICS OF THE ERS-1 PRI AND JERS-1 LEVEL 2.1 PRODUCT [22], [32]

	ERS-1 Precision Image	JERS-1 Level 2.1
Georeferenced	yes	yes
Antenna pattern corrected	yes	yes
Corrected for range-spreading loss	yes	yes
Corrected for local incidence angle	no	yes (based on ellipsoid)
Number of Looks	3	3
SAR geometry	ground range	ground range
Pixel spacing range/azimuth	12.5 m	12.5 m
Scene area range	100 km	75 km
Scene area azimuth	~ 102.5 km	80 km
Range pixels	8000	6000
Azimuth pixels	~ 8200	6400

The scenes delivered from the German Processing and Archiving Facility (ERS-1) and the Japanese RESTEC (JERS-1) were the Precision Image (ERS-1) and Level 2.1 (JERS-1) product, with their characteristics listed in Table V. Both products are processed at three looks, delivered in ground range projection with 12.5-m pixel spacing, and corrected for their specific antenna pattern and range-spreading loss. An ellipsoid-based local incidence angle correction of the area term is done for the JERS-1 Level 2.1 products.

4) Orthorectification: Due to the SAR inherent geometric distortions during image acquisition, it is necessary to use height information for the geometric correction of pixel displacements in range (across track) and azimuth (along track) direction.

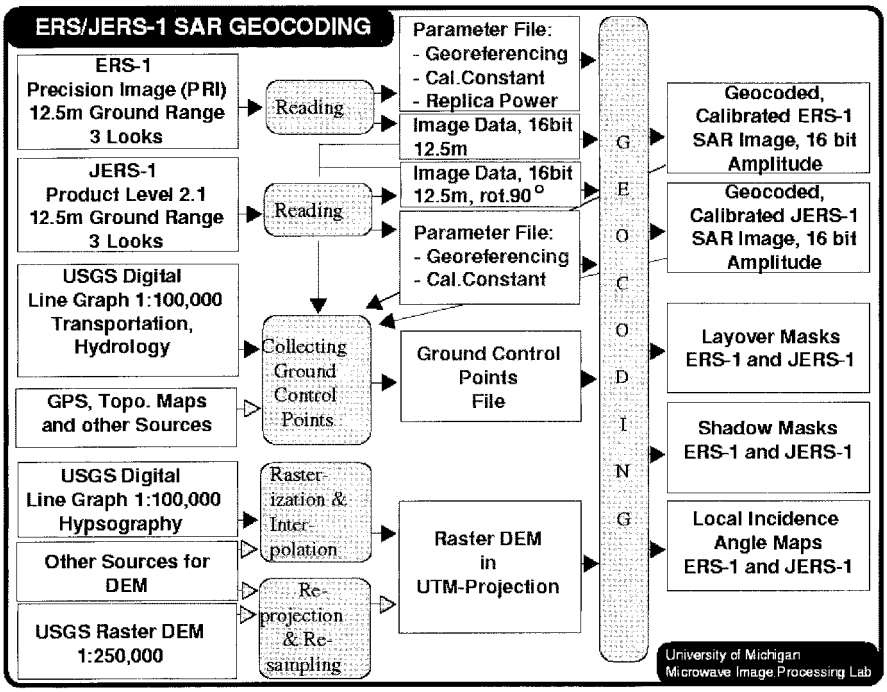

Fig. 2. Flowchart of the orthorectification process to generate ERS-1/JERS-1 composites.

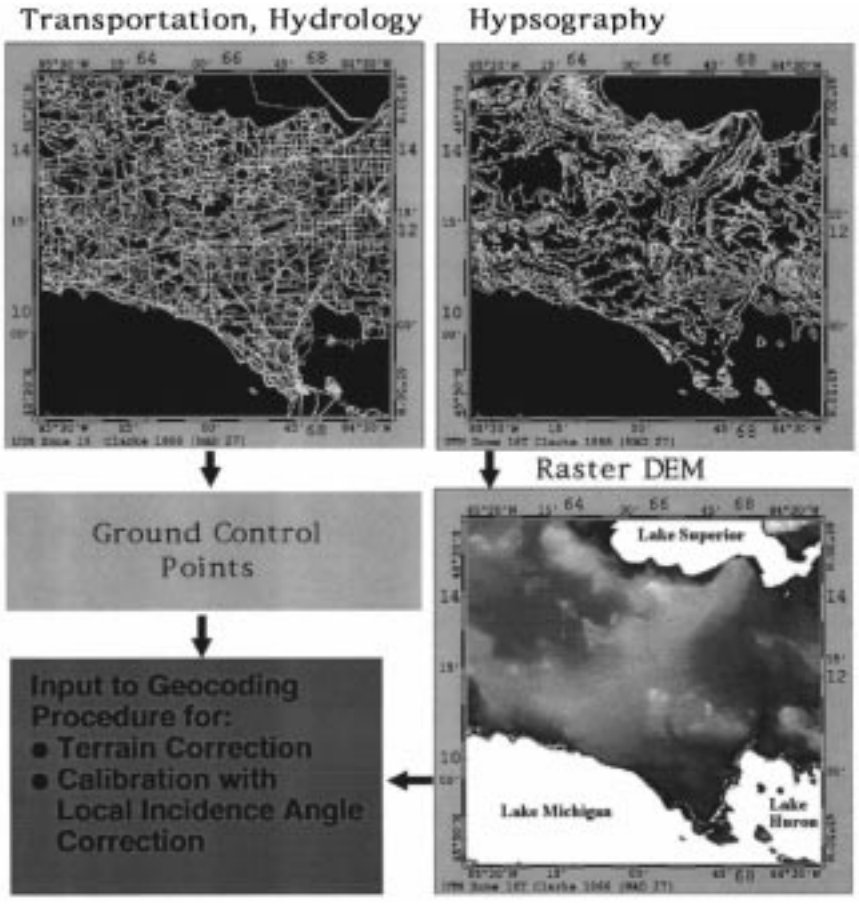

Fig. 3. USGS DLG data 1:100 000 used for the generation of raster DEM's and the collection of GCP's.

The geometric quality of the orthorectification process is determined by the accuracy of the orbit information and the digital elevation model (DEM). Ground control points (GCP's) are needed since the orbit information does not provide absolute ephemeris data. It was experienced that a minimum of four GCP's was sufficient

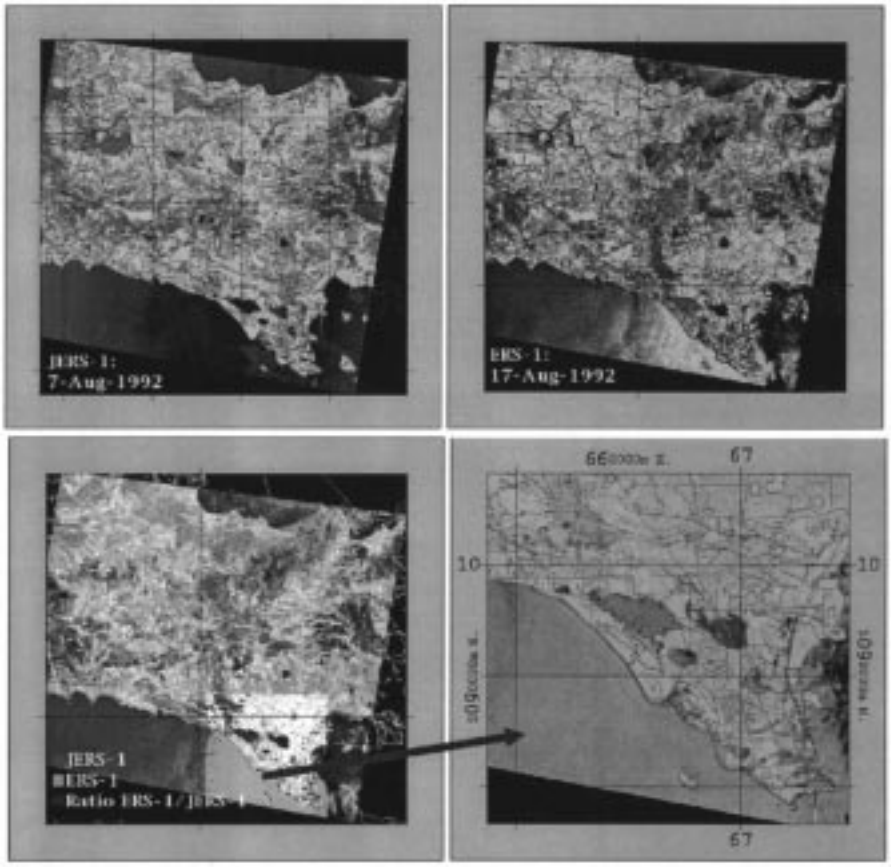

Fig. 4. Orthorectified ERS-1 (Aug. 17, 1997) and JERS-1 (Aug. 7, 1997) scenes of the test site Raco.

for refinements of the orbit information and first-order point transformations during the final orthorectification run [17]. Generally, the GCP's were collected using United States Geological Survey (USGS) 1 : 100 000 Digital Line Graph (DLG) data and Global Positioning System (GPS) measurements. For all but the Cabaliana test site, the USGS 1 : 100 000 hypsography DLG data could be used to generate 25-m pixel spacing raster DEM's after an algorithm published by [18] (Fig. 3). Since height differences in the Cabaliana test site were fairly small, ellipsoid-based geocoding showed satisfactory accuracy (validated visually). For all other test sites, the achieved geometric accuracy was less than two pixels (25-m spacing) on average (e.g., Fig. 4), which was considered sufficient for the purpose of vegetation classification at regional-to-global scale. However, experimental use of USGS 1 : 250 000 DEM raster data resulted in much worse accuracies and almost no layover or shadow regions could be detected using this coarse-resolution DEM.

5) Radiometric Calibration: The radiometric calibration of the ERS-1 and JERS-1 imagery is another critical preprocessing step, considering the intention of multisite classification using a classifier based on absolute backscattering values.

Considerable progress has been made in the calibration of SAR imagery in recent years [19], [20]. For ERS-1 and JERS-1, accuracies have been reported to be on the order of 0.5 dB [21], [22].

Since the delivered ERS-1 precision image (PRI) scenes are corrected for antenna pattern and range-spreading loss by the processing facility, the correction for local incidence angle and image replica power adjustment needed to be done using the following equation (after [16], [23]):

$$I = \frac{DN_{\text{in}}^2}{K} \frac{\sin(\alpha_{\text{DEM}})}{\sin(\alpha_{\text{ref}})} \frac{\text{IRP}}{\text{RRP}} \tag{1}$$

where

I	intensity;
DN_{in}	digital number of input image file;
K	calibration constant;
α_{DEM}	local incidence angle calculated from the DEM;
α_{ref}	reference incidence angle (23°);
IRP	image replica power;
RRP	reference replica power (205 229).

For JERS-1, no replica power adjustment is necessary since JERS-1 has an *automatic gain control* (AGC) onboard. Unlike the ERS-1 PRI data, the JERS-1 Level 2.1 SAR images are already corrected for the local incidence angle [22], [24]. Since this is done for an ellipsoidal surface and not for the true local angle of incidence, as derived from a DEM, calibration of the JERS-1 SAR data is performed as follows. Assuming the local incidence angle correction for the ellipsoid was done using the term $\sin(\alpha_{\text{ELL}})/\sin(\alpha_{\text{ref}})$, the following equation was to be

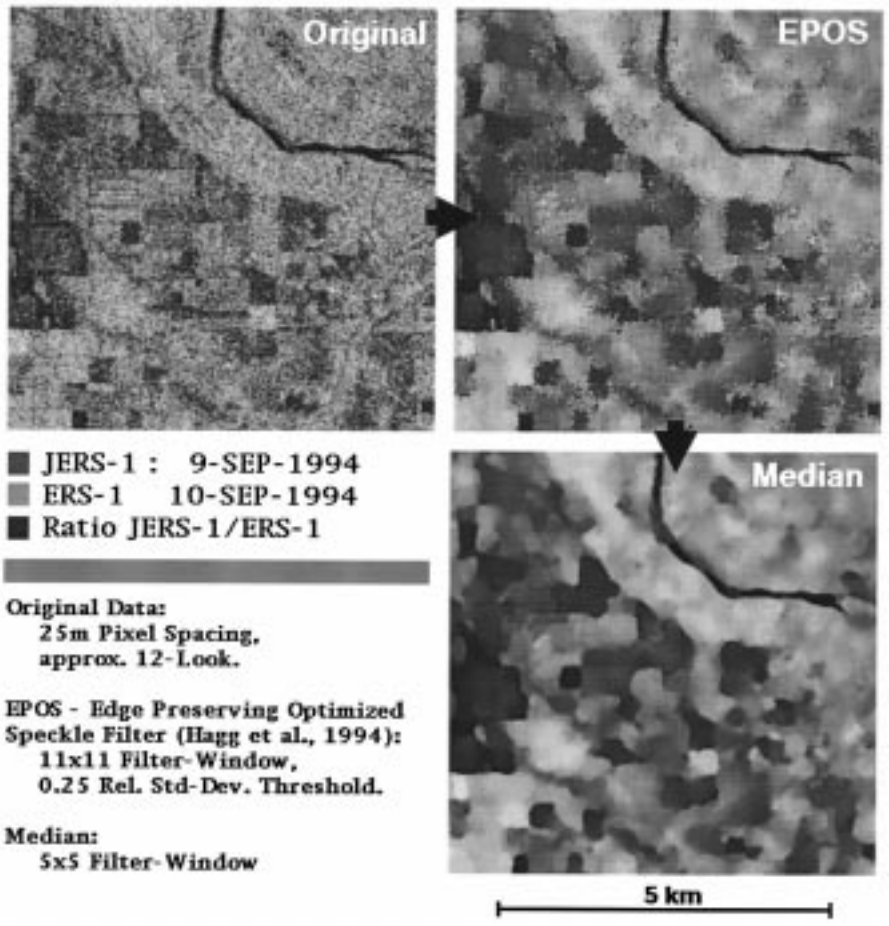

Fig. 5. Application of the EPOS and median filter in the radiometric preprocessing of the ERS-1/JERS-1 composites. Note the removal of speckle noise through the EPOS filter and the further removal of point targets and edge noise through the consequent application of the median filter. Although some smoothing can be seen, the process preserves edges to a very high degree. The image subset is taken from the Cedar Creek ERS-1/JERS-1 composite.

applied to calibrate the JERS-1 data:

$$I = \frac{DN_{\text{in}}^2}{K} \frac{\sin(\alpha_{\text{DEM}})}{\sin(\alpha_{\text{ELL}})} \tag{2}$$

where, α_{ELL} = local incidence angle calculated from the Ellipsoid.

In summary, the following conclusions can be stated for the radiometric correction of ERS/JERS imagery.

- Shadow occurs almost never in ERS-1 images, whereas layover regions are of greater extent in ERS-1 than in JERS-1 scenes.
- Corrections of the illuminated area due to slope are more critical in ERS-1 than in JERS-1 images.

Both effects are due to the lower incidence angle of the ERS-1 SAR (see Table I).

6) Radiometric Upgrading: The first step in the process to reduce fading (speckle) is the application of the EPOS filter, which was designed to preserve edges while reducing the noise in homogeneous areas to a very high degree. To further remove point targets (e.g., vehicles, power masts, antennas, etc.) and to clean noisy edges, a 5×5 median filter was applied to the image composites subsequently. This resulted in fairly smooth image data, in which large segments dominate over finer structures that are still preserved to a certain degree (Fig. 5). Visual interpretation of the filtered JERS-1 imagery shows that features on the order of two to three 25-m pixels for JERS-1 and two to four 25-m pixels for ERS-1 are still separable. This translates into estimates for the effective resolution for ERS-1 of 50–100 m and for JERS-1 of 50–75 m after filtering. This is significantly better than estimates on the order of 200 $\times$ 200 m given by [26]. Important for the purpose of radar signature generation and comparison was that the filtering process would preserve the mean estimate of distributed targets, i.e., homogenous vegetation units should have quasi-identical σ°-values before and after filtering. This was achieved together with a reduction of the $\pm 1\sigma$ variance around the mean backscatter from 5 dB to 0.1 dB (Fig. 6). Since the total dynamic range of the imagery is on the order of roughly 20 dB, significant noise reduction is important. As a last step in the data preprocessing for reasons of data reduction and approach to a Gaussian distribution, the amplitude values were converted to decibels and represented in 8 bit with $0\text{–}255 = -25 - +0.5$ dB. Hence, each digital number represents a 0.1-dB step. Given the achieved calibration accuracies and the dynamic range of vegetation cover, this was considered sufficient. The standard

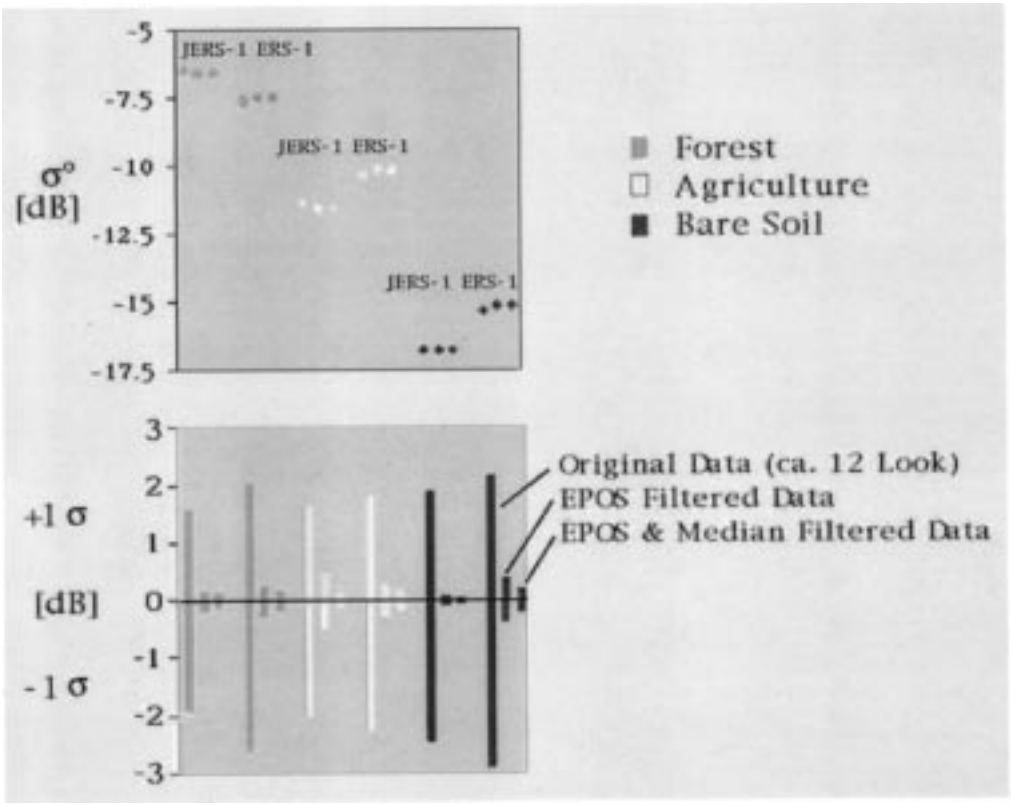

Fig. 6. Retention of the mean and reduction of the signal variance throughout the filtering process for various vegetation categories measured from both ERS-1 and JERS-1 SAR data. The radiometric $\pm 1\sigma$ variance of $\sim$5 dB in the original image is reduced by a factor of ten to approximately 0.5 dB in the resulting filtered product.

way to display the composites was chosen to be JERS-1 in red, ERS-1 in green, and the decibel difference channel ERS-1–JERS-1 in blue.

7) ERS-1/JERS-1 Composites: Fig. 7 shows the resulting JERS-1 composites after applying geometric and radiometric calibration and speckle noise reduction. The chosen channel selection for the false-color display is

Red:	L_{hh}	$(\text{JERS} - 1)$
Green:	C_{vv}	$(\text{ERS} - 1)$
Blue:	$C_{vv} - L_{hh}$	$(\text{ERS} - 1\text{–JERS} - 1)$.

All images were digitally enhanced using histogram equalization. Hence, during visual comparison of the composites, it has to be considered that similar colors in different sites do not necessarily reflect similar class categories since different gray-value stretching in the various channels of the composites occurred. However, general trends can be identified and compared. Dark **blue** colors show regions where both ERS-1 and JERS-1 values are low, with ERS-1 values still slightly higher than JERS-1. This is a typical appearance of low biomass regions, e.g., grassland (Konza Prairie [Fig. 7(d)]) and desert grass/shrubland (Jornada [Fig. 7(b)] and Sevilleta [Fig. 7(g)]). Also, water bodies appear generally blue since the JERS-1 return is close to the noise level, while ERS-1 shows mostly moderate backscattering values due to the C_{vv} sensitivity to the water surface roughness. Examples are the Great Lakes in the Raco scene [Fig. 7(f)] and the Rio Solimões and adjunct water bodies in the Cabaliana scene [Fig. 7(a)]. **Light blue** colors dominate in cases in which low JERS-1 backscatter is coupled with medium-to-high ERS-1 values. This occurs in rough water areas as well as some wetland areas; e.g., Raco (660 000 E, 5 128 000 N), where L_{hh} penetrates into the canopy and specular scattering dominates the total return, while C_{vv} shows a strong moisture-related backscatter. **Yellow** colors indicate high backscatter values for both ERS-1 and JERS-1 and usually can be related to high biomass regions. Also, forested wetlands (Cabaliana, Raco) and riparian forests (Konza) are typically presented in this color. The vegetation structural differences are most significantly represented by **red** colors, which indicate high JERS-1 values and low ERS-1 values. This combination is typical for needleleaf excurrent tree forms and can be found throughout the Raco, Kellogg [Fig. 7(c)], and Cedar Creek site [Fig. 7(e)]. **Cyan** colors are typical for agricultural areas since the ERS-1 backscatter of rough soils, irrigated land, and mainly corn crops is much higher than the JERS-1 values, e.g., Kellogg, Cedar Creek, and the western part of the Konza composite.

V. Classification

A. Hybrid Unsupervised/Supervised Approach

With the goal of automating the process of vegetation classification from SAR data, the chosen algorithm should minimize user interaction. Also, based on the new develop-

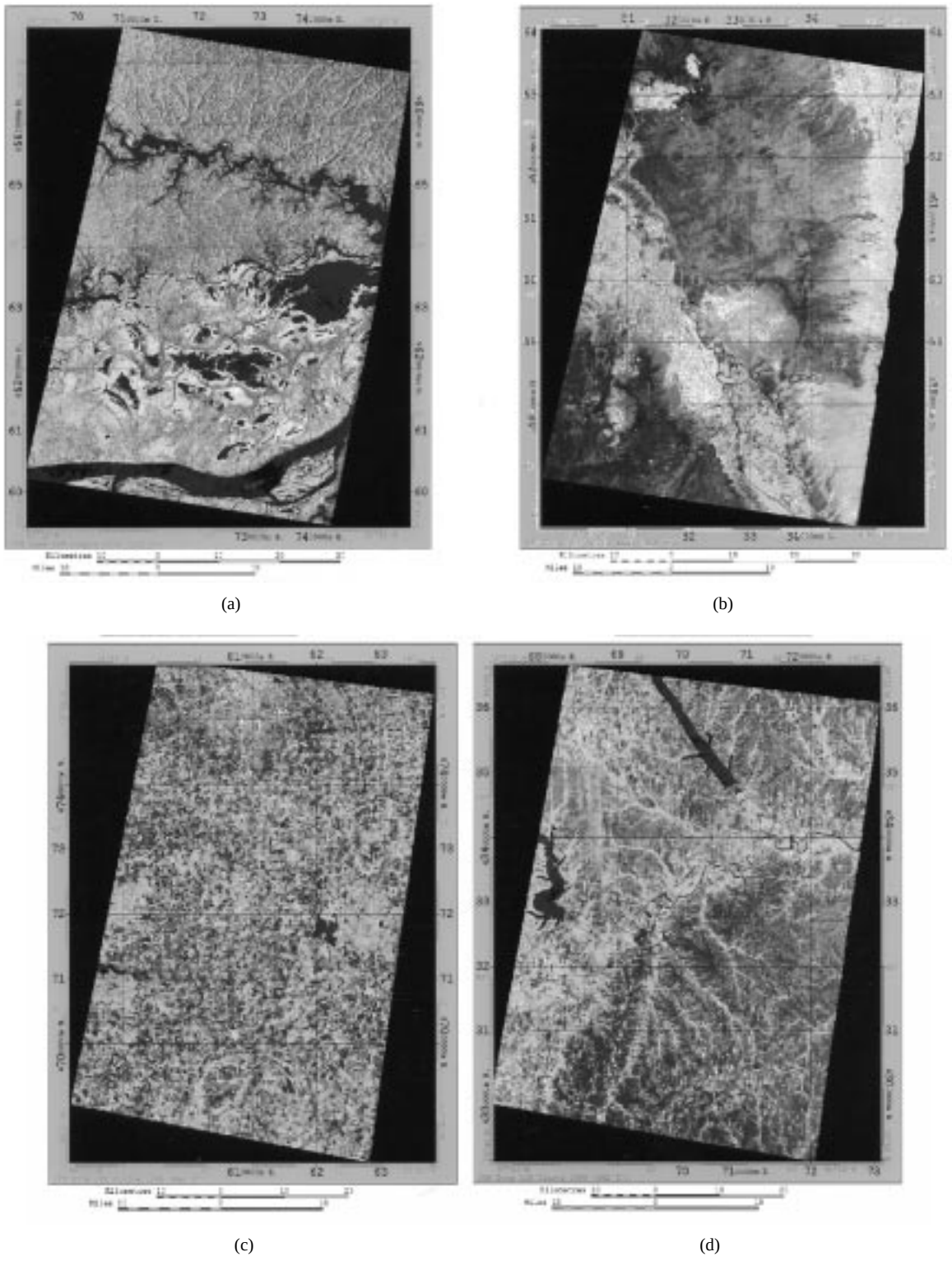

(a) (b)

(c) (d)

Fig. 7. ERS-1/JERS-1 composites of the test sites (a) Cabaliana (tropical rain forest), (b) Jornada (shrub desert), (c) Kellogg (temperate forest and agriculture), and (d) Konza Prairie (tallgrass prairie). The channel selection is red $= L_h h\sigma^\circ$ JERS-1, green $= C_v v\sigma^\circ$ ERS-1, and blue = ERS-1–JERS-1 (dB-difference).

ments in accurate SAR data calibration, the possibility of defining classification rules based on *backscatter signatures* was postulated. Similar to classification approaches using global remote-sensing data sets created from the National Oceanic and Atmospheric Administration (NOAA) Advanced Very High Resolution Radiometer (AVHRR) data [27], [28], an unsupervised classification method was chosen as the initial step to cluster data in the spectral domain. Fig. 8 describes the hybrid unsupervised/supervised approach that was pursued at this stage.

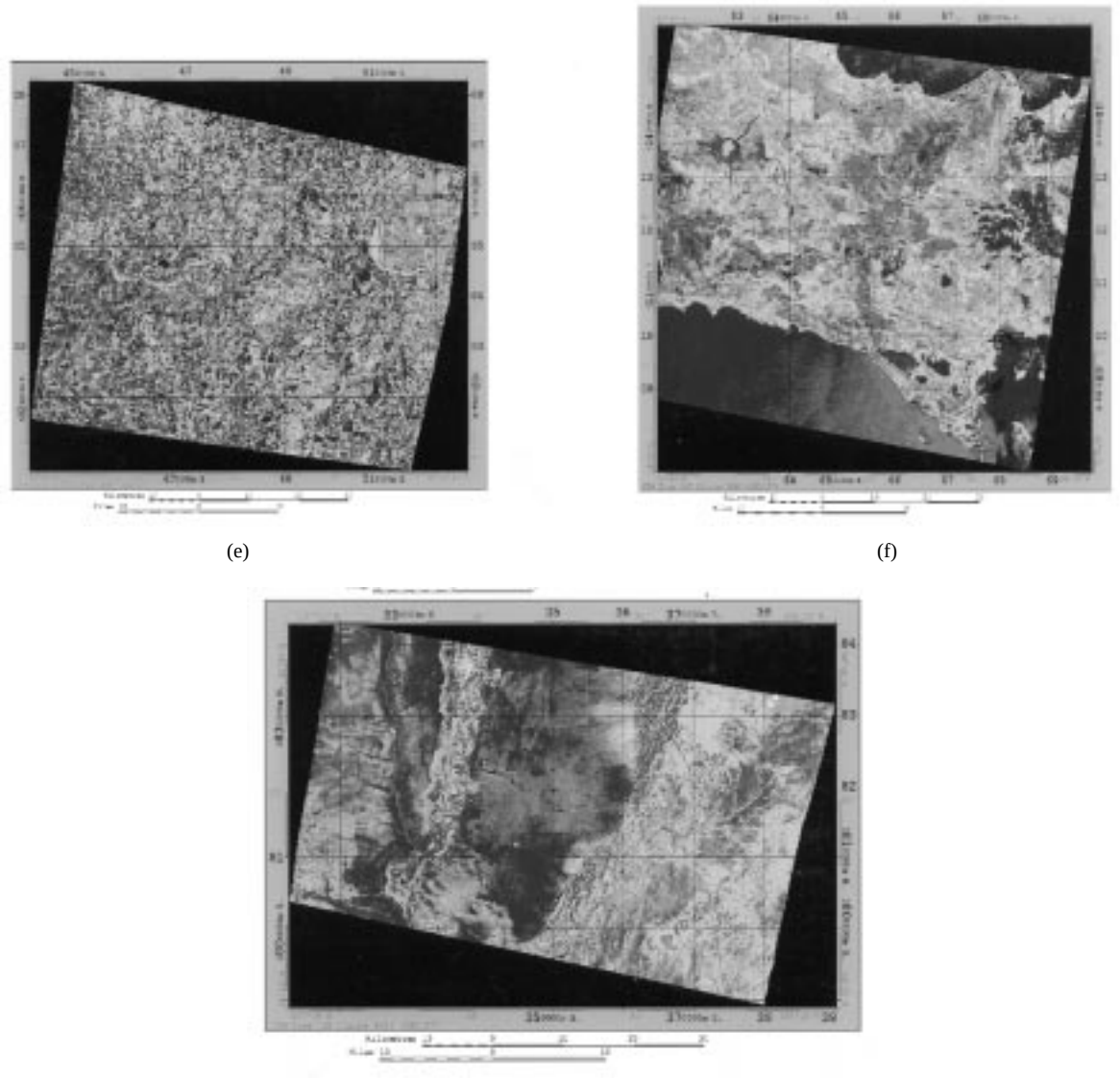

(e) (f)

(g)

Fig. 7. (*Continued.*) ERS-1/JERS-1 composites of the test sites (e) Cedar Creek (transition prairie/midlatitude forest), (f) Raco (transition zone temperate forest/boreal forest), and (g) Sevilleta (shrub desert). The channel selection is red = $L_h h\sigma^\circ$ JERS-1, green = $C_v v\sigma^\circ$ ERS-1, and blue = ERS-1–JERS-1 (dB-difference).

Using the ISODATA algorithm [29], each image composite was clustered (unsupervised) and cluster signatures were calculated.

With the minimum-distance rule, the cluster signatures $\vec{m}_c$ from all test sites were classified using the measured signatures from all training polygons (P).

For each test site, the classification was done using the set of polygons measured in all test sites

$$Class_{\vec{m}_{c_{site}}} = Class_{\vec{m}_p} \tag{3}$$

where p is determined from

$$\min\left[||\vec{m}_{c_{site}} - \vec{m}_p||\right]_{p=1}^{P}$$

with

site $= 1, \cdots,$ total number of test sites (here: seven);
$p = 1, \cdots,$ total number of measured polygons;
$\vec{m}_{c_{site}}$ result of ISOCLASS for test site *site*;
$\vec{m}_p$ $(\sigma^\circ_{\mathrm{JERS_p}}, \sigma^o_{\mathrm{ERS_p}})$.

The method described above can be considered fairly simple, no other possible features (e.g., texture) are used, and the classification is straightforward and leads to automated and unsupervised-defined radar backscatter signatures that can be used as a classification basis. The advantage of this approach is the possibility of using one set of signatures for multiple sites, while retaining the flexibility of cluster naming using additional data sources like ecoregion maps, DEM's, or other satellite imagery [30]. Also, simple calibration adjustments or physically derived shifts due to moisture changes can be imposed equally on cluster and backscatter signatures even after the clustering procedure.

Since the focus of this study was on the classification of vegetation structural classes, and since urban and water areas

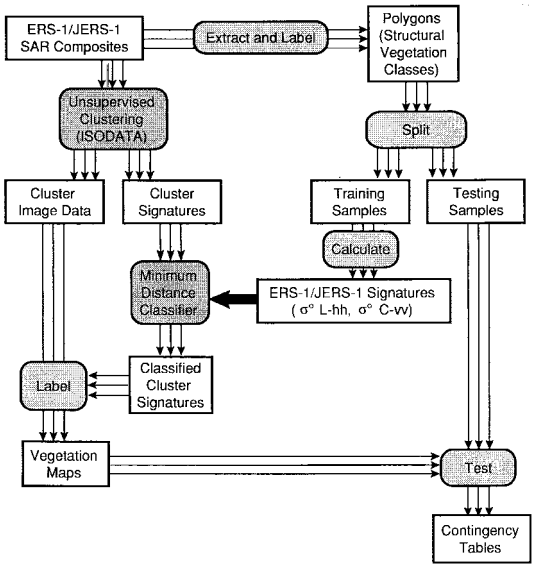

Fig. 8. Overview over the hybrid unsupervised/supervised classification of ERS-1/JERS-1 composites.

are difficult to classify on the basis of backscatter only with ERS-1 and JERS-1, it was decided to mask urban and water areas prior to the unsupervised clustering with ISODATA. The urban and water areas were derived from the existing USGS *land use/land cover* (LULC) database in all six United States test sites. No larger urban areas were present in the test site Cabaliana, and the water mapping seemed possible from the JERS-1 data alone by simple thresholding at −12.5 dB after unsupervised classification.

VI. Results

All accuracy metrics were derived from testing populations which were one-half of the total polygon samples and created by splitting each polygon in two equal-sized upper and lower sections.

1) Multisite Classification: The results of the ISODATA clustering for each test site composite is shown in Fig. 9. It is already interesting to interpret Fig. 9 just on the basis of test site location and major vegetation inventory. The diameter of a circle represents the relative number of pixels assigned to that cluster represented by its midpoint in the ERS-1/JERS-1 scattergram. As expected, forested sites (Cabaliana, Cedar Creek, Kellogg, and Raco) show the bulk of samples in the high backscatter regions (upper right), whereas generally deforested sites (Jornada, Konza Prairie, and Sevilleta) have more cluster centers in the low backscatter region (lower left). However, the trend to horizontal distribution of the clusters with many pixels assigned (e.g., Sevilleta, Cedar Creek, but also Raco and Konza Prairie) is an indication of the larger dynamic range of JERS-1 (L-band) for vegetation observation. Generally, the unsupervised, generated plots also show the dynamic ranges of both sensors for vegetation observation to be on the order of −18 to −4 dB.

Fig. 10 shows the measured ERS-1/JERS-1 signatures measured from polygons in all test sites. The fairly good separation

TABLE VI
Summary of the Accuracy of the Level 1 Classification for all Test Sites. The Three Level 1 Classes Are Woody, Herbaceous, and Mixed/Herbaceous. All Accuracies Are Expressed in Percent

Test Site	Testing Samples	Area (ha)	Mean User Accuracy	Mean Producer Accuracy	Kappa Index	Overall Accuracy
Cabaliana, Brazil	5856	366	78.4	87.1	0.38	76.6
Sevilleta, New Mexico	232	15	65.6	46.5	0.22	68.4
Jornada, New Mexico	463	29	41.2	62.1	0.44	80.4
Konza Prairie, Kansas	1644	103	90.3	97.4	0.86	97.6
Cedar Creek, Minnesota	478	30	81.6	74.7	0.47	69.0
Kellogg, Michigan	258	16	99.7	99.4	0.99	99.6
Raco, Michigan	4954	310	84.0	86.7	0.89	93.9
All Sites	13855	866	66.5	76.5	0.73	85.5

TABLE VII
Summary of the Accuracy Assessment of the Level 2 Classification for all Test Sites. All Accuracies Are Expressed in Percent

Test Site	Testing Samples	Area (ha)	Mean User Accuracy	Mean Producer Accuracy	Kappa Index	Overall Accuracy
Cabaliana, Brazil	5856	366	41.9	43.3	0.41	58.0
Sevilleta, New Mexico	232	15	52.6	35.1	0.23	68.4
Jornada, New Mexico	463	29	54.8	68.7	0.70	80.2
Konza Prairie, Kansas	1644	103	95.1	97.0	0.86	97.6
Cedar Creek, Minnesota	478	30	76.4	50.5	0.37	56.7
Kellogg, Michigan	258	16	94.5	71.1	0.63	72.0
Raco, Michigan	4954	310	62.7	64.4	0.72	82.3
All Sites	13855	866	54.7	53.1	0.63	72.5

for level 1 classes (woody, herbaceous, and mixed) is mainly driven by JERS-1. At level 2, distinction between needleleaf and broadleaf as well as wetland classes is introduced mainly through ERS-1 backscatter characteristics and follows the conceptual model postulated by [5]. However, ambiguities exist, especially between the classes in the transition zone of different biomass levels, like shrubland/tree canopy and shrubland/herbaceous. Also, needleleaf wetland forests and wet shrubs (Cabaliana) are generally confused with deciduous forests. These distinctions seem fairly difficult to resolve with just the two like-polarized sensors and monotemporal analysis. To test the limits of this approach, the clusters were classified using the backscatter signatures without any alterations or adjustments. The results for the level 1 and 2 multisite classification are shown in Tables VI and VII.

2) Multitemporal Classification: Since it became evident that monotemporal (i.e., same season) composites have some inherent class ambiguities, multitemporal data were added to the ERS-1/JERS-1 feature vector. However, this was only done for the Raco test site at this stage. The trend of improvement in accuracy and kappa index can be seen from the results for both Level 1 (Table VIII) and Level 2 (Table IX) when fall (JERS-1) and winter (ERS-1) scenes are added to the process. A more detailed description of the multitemporal study is found in [31] and planned for a follow-up publication.

VII. Sensitivity to Backscatter Changes

The sensitivity of the classifier to uncertainties in the backscattering values was tested with 441 classification runs, varying the unsupervised generated cluster means from −2 to

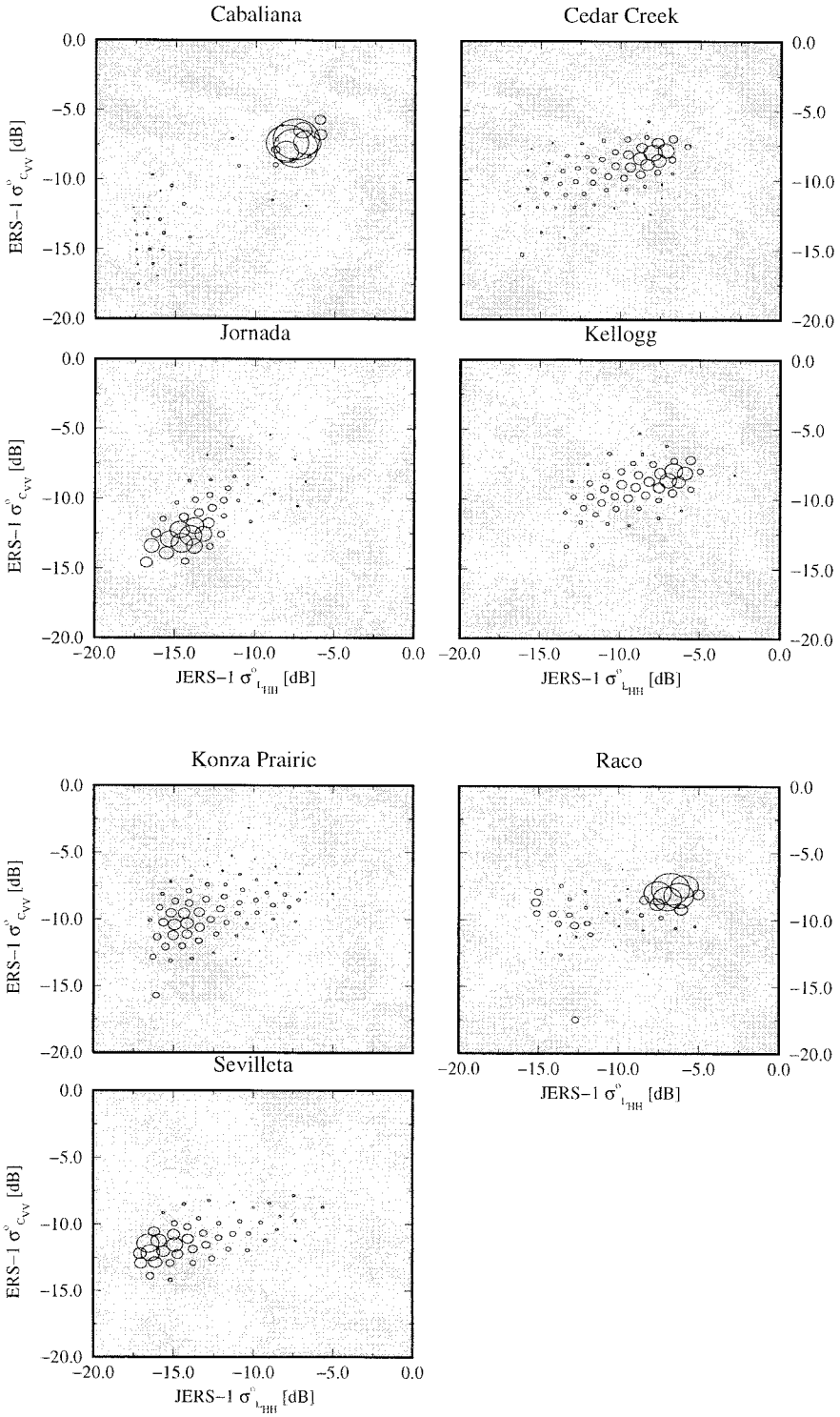

Fig. 9. Result of ISOCLUS for the test sites. The midpoints of the circles represent the cluster centers $\vec{m}_c$. The radius represents the relative percent area (number of pixels) that is classified to that cluster.

+2 dB in 0.2-dB steps around the originally calculated cluster means. The JERS-1-signatures were kept constant.

The results of this simulation are shown in Fig. 11. From this simulation, it can be seen that the level 1 classification results are mainly sensitive to changes in the JERS-1 backscattering values, with the main drop in accuracy at approximately ±1 dB. However, at level 2, the significant drop in classification accuracies is caused by both sensors equally at about ±0.5 dB.

VIII. Discussion

Concerning the overall results of the multisite study, it has to be considered that great care was taken in selection of the

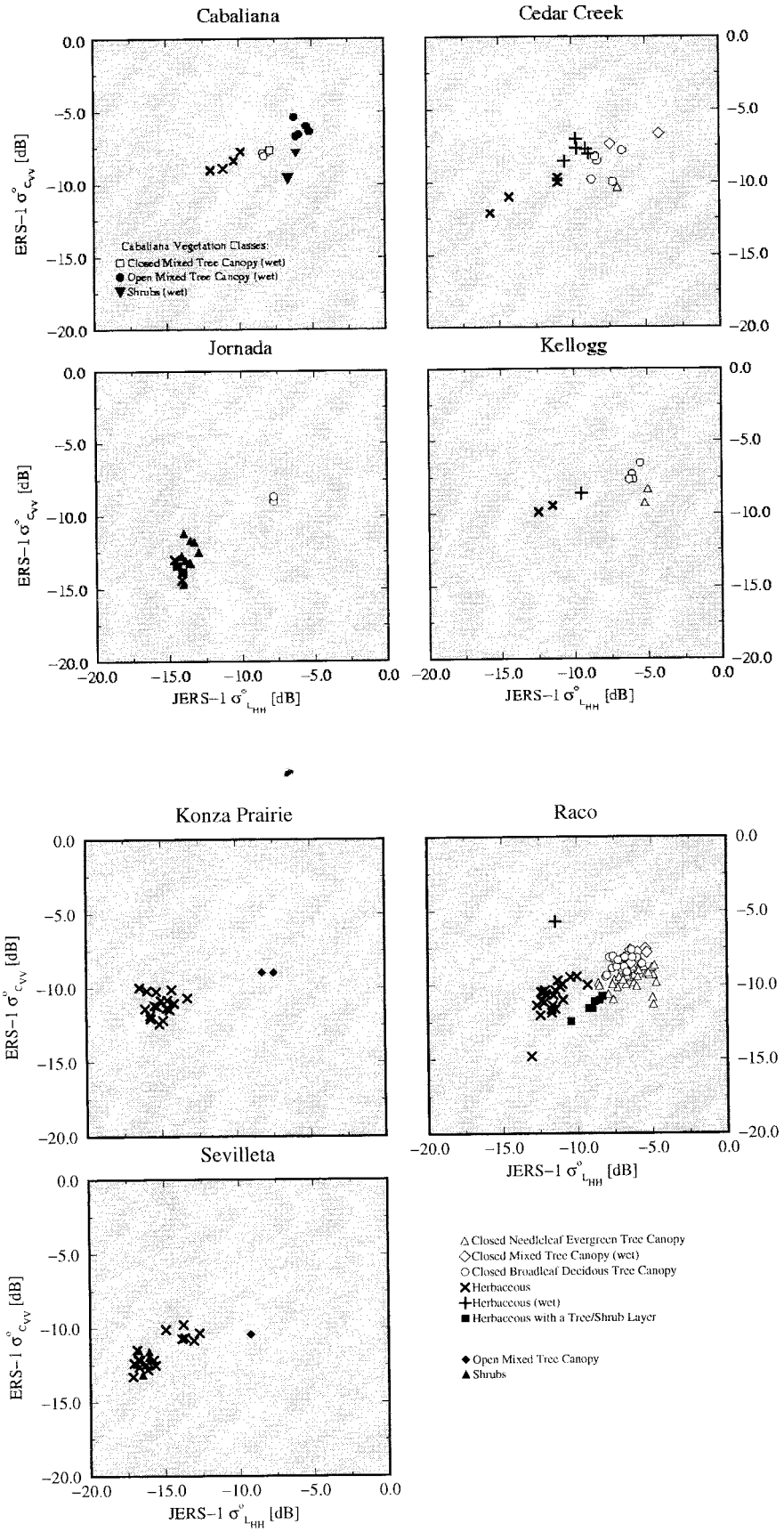

Fig. 10. Measured ERS-1/JERS-1 backscatter values from polygons of various vegetation structures in the test sites. Left to right, top to bottom: Cabaliana, Cedar Creek, Jornada, Kellogg, Konza, Raco, Sevilleta.

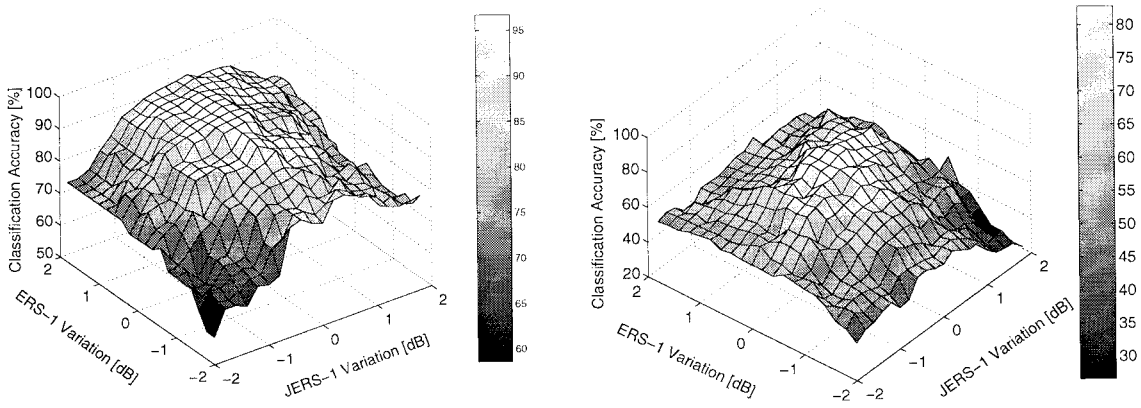

Fig. 11. Dependency of the classification accuracy on the variance (sensor calibration and/or land-cover changes) of the backscattering coefficient σ^o from ERS-1 and JERS-1. Left: Level 1, indicating a strong dependency on L-band. Right: Level 2, indicating a dependency on both C- and L-band.

TABLE VIII
SUMMARY OF THE ACCURACY ASSESSMENT OF THE LEVEL 1 CLASSIFICATION FOR MULTITEMPORAL AND MULTISENSORAL COMBINATIONS IN THE TEST SITE RACO. ALL ACCURACIES ARE EXPRESSED IN PERCENT

Classification Input	Mean User Accuracy	Mean Producer Accuracy	Kappa Index	Overall Accuracy
ERS-1 August	48.1	43.6	0.17	43.5
JERS-1 August	73.2	79.4	0.79	88.4
ERS-1 + JERS-1 August	86.4	79.4	0.90	94.6
Both August + JERS-1 October	82.4	87.6	0.88	93.6
Both August + ERS-1 January	88.7	83.1	0.89	94.3
Both August + JERS-1 Oct. + ERS-1 Jan.	93.8	83.3	0.90	94.9

TABLE IX
SUMMARY OF THE ACCURACY ASSESSMENT OF THE LEVEL 2 CLASSIFICATION FOR MULTITEMPORAL AND MULTISENSORAL COMBINATIONS IN THE TEST SITE RACO. ALL ACCURACIES ARE EXPRESSED IN PERCENT

Classification Input	Mean User Accuracy	Mean Producer Accuracy	Kappa Index	Overall Accuracy
ERS-1 August	30.2	36.6	0.16	29.8
JERS-1 August	45.8	49.2	0.52	66.3
ERS-1 + JERS-1 August	71.9	70.7	0.73	81.2
Both August + JERS-1 October	79.1	84.0	0.81	86.3
Both August + ERS-1 January	83.4	82.6	0.83	87.8
Both August + JERS-1 Oct. + ERS-1 Jan.	84.6	82.1	0.83	87.8

scenes and calibration during preprocessing. Hence, the relatively good classification result was achieved under "optimum" conditions. However, the per-site results indicate the sensitivity of a signature-based classifier to backscatter variations that can be related to both natural effects and system calibration uncertainties. The simulation study of accuracy dependency on backscatter change suggests that system calibration must be better than 0.5-dB absolute—a challenge to engineers that is partly met by today's systems. Generally, calibration of SAR systems is becoming more and more accurate and reliable, while natural conditions are only stable to a certain degree. Since moisture changes can alter the backscattering signal significantly, tropical environments in particular might show different backscattering behavior than other ecoregions. An ecoregional moisture-related backscatter gradient can only be speculated at this point, based on few measurements in the Cabaliana test site compared with the other scenes, where mainly ERS-1 measurements of comparable structural classes seem generally higher than in the other test sites. However, whether this effect is related to calibration uncertainties or biomass differences remains a subject of discussion.

Consequently, the successful multisite classification achieved with the data set in seven test sites does not result in a ready, applicable classifier that would work to satisfaction everywhere and anytime given two ERS-1 and JERS-1 scenes. This is as expected. Nonetheless, the result of the multisite study is seen as a proof of the following principle: it is possible to combine L- and C-band SAR data from two existing orbital systems and extract more valuable information from the combined backscatter signatures than from either sensor taken alone. Furthermore, it was shown that indeed similar structural classes show similar, separable backscatter signatures, no matter in which test site they were measured. This leads to the postulation that radar signature-based classification is possible.

At this point of research, only recommendations can be given on how the unknown backscatter variations can be addressed in a universally applicable classifier realization. A constant offset in data due to calibration uncertainties might be addressable by an "adaptive signature classifier." If the calibration bias is known, the signatures can be adjusted by adding or subtracting the bias from the corresponding part of each signature. With some training/testing polygons available, the adjustment could also be realized in form of an "autofocus" classifier, meaning the signatures are adjusted in increments until the classification result is optimized.

The proposed hybrid classifier would be very flexible in this respect since the time-consuming unsupervised clustering must only be executed once, and the autofocus correlation is performed only on the cluster and backscatter signatures.

With increased research and applications using spaceborne SAR systems, more and more backscatter signatures become available and the compilation of signature databases including very detailed ground-truth data, such as biometric data, moisture conditions, phenological stage, underlying soil type,

etc., will evolve. Hence, sets of backscatter signatures for classification could be defined that are specific for ecoregion and environmental conditions. With some *a priori* knowledge, the right set of signatures can thus be selected for classification. The incorporation of geographic knowledge in the process should be assessed. Clearly, more research is needed to define the limits and potential of these scenarios.

IX. Concluding Remarks

The potential of the combination of the ERS-1 C_{vv} and JERS-1 L_{hh} bands for large-scale vegetation classification on a structural basis has been demonstrated in the multisite classification study. The power of combining existing SAR systems of different frequencies was clearly demonstrated by the classification results using multitemporal combined ERS-1/JERS-1 data in the test site Raco. Level 2 accuracies above 80% in all accuracy metrics based on a decent number of testing samples can be considered a major contribution to regional-scale vegetation classification with respect to guaranteed data availability. More research is needed in using multitemporal combined ERS-1/JERS-1 data in different environments with a broader range of vegetation inventory.

Steady improvements in SAR calibration and image analysis techniques clearly support the move toward a globally consistent vegetation characterization tool complimentary to optical systems. Recalling Table II, it can be concluded, that orbital SAR systems are very well suited to play a key role in global monitoring of vegetation structural classes, as defined by TOPC, especially when more capable SAR systems, like Envisat/ASAR (C-band vv, hh, hv, and vh), ALOS/PALSAR (L-band hh, and vv), and LightSAR (L-band polarimetric $+X/C$-band), are deployed into space. A thorough exploration of the integration of optical and SAR systems is urgently needed.

Acknowledgment

The authors thank all collaborators for their support in the acquisition of ground truth and discussion of polygon labels: K. Bergen, The University of Michigan, Ann Arbor, L. Huenneke, B. Nolen, New Mexico State University, Las Cruces, L. Hess, University of California, Santa Barbara, J. Briggs, G. Hennebry, Kansas State University, Manhattan, P. Bolsted, P. Reich, University of Minnesota, Minneapolis, S. Halsted, P. Robertson, S. Hamilton, L. Krievs, Kellogg Biological Station, MI. Further acknowledged are W. Hagg and M. Sties, University of Karlsruhe, Germany, for the EPOS filter and L. Norikane and J. Curlander, Vexcel Corporation, Boulder, CO, for parts of the geocoding software.

References

[1] Terrestrial Observation Panel for Climate (TOPC), "GCOS/GTOS plan for terrestrial climate-related observations," WMO/UNEP/UNESCO/FAO/ICSU, Tech. Rep. GCOS-32, WMO/TD, no. 796, June 1997.

[2] M. C. Dobson, F. T. Ulaby, and L. E. Pierce, "Land-cover classification and estimation of terrain attributes using synthetic aperture radar," *Remote Sens. Environ.*, vol. 51, pp. 199–214, Jan. 1995.

[3] T. Le Toan, "Assessment of ERS-1 SAR data for forest studies in Southeast Asia," *ESA Earth Observ. Quart.*, no. 48, June 1995.

[4] Centre Nationale d'Études Spatiale, Ed., *Retrieval of Bio- and Geophysical Parameters from SAR Data for Land Applications*, Centre Nationale d'Études Spatiale, Toulouse, France, Oct. 13–15, 1995.

[5] M. C. Dobson, L. E. Pierce, and F. T. Ulaby, "Knowledge-based land-cover classification using ERS-1/JERS-1 SAR composites," *IEEE Trans. Geosci. Remote Sensing*, vol. 34, pp. 83–99, Jan. 1996.

[6] L. L. Hess, J. M. Melack, S. Filoso, and Y. Wang, "Delineation of inundated area and vegetation along the Amazon floodplain with SIR-C synthetic aperture radar," *IEEE Trans. Geosci. Remote Sensing*, vol. 33, pp. 896–904, July 1995.

[7] Federal Geographic Data Committee, Vegetation Subcommittee, "FGDC vegetation classification and information standards," FGDC Secretariat, USGS, Reston, VA, June 1996.

[8] J. M. Kellndorfer, M. C. Dobson, and F. T. Ulaby, "Multi-ecoregion vegetation mapping using combined ERS/JERS SAR imagery," in *Proc. 3d ERS Symp.*, Eur. Space Agency, Mar. 1997.

[9] J. M. Kellndorfer, R. Schadt, and W. Mauser, "Segmented landuse classification of multi-temporal ERS-1 SAR data," in *Proc. 1st ERS Symp.*, Eur. Space Agency, ESA-SP 359, Nov. 1992, pp. 532–536.

[10] ———, "The use of multitemporal ERS-1 SLC data for landuse classification," in *Proc. IEEE Int. Geosci. Remote Sensing Symp. (IGARSS'93)*, Tokyo, Japan, pp. 1608–1610.

[11] J.-P. Malingreau and G. Duchossois, "The TREES/ERS-1 SAR '94 project," *ESA Earth Observ. Quart.*, no. 48, June 1995.

[12] C. Schmullius and A. Rosenquist, "Closing the gap—a Siberian boreal forest map with ERS-1/2 and JERS-1," in *Proc. 3rd ERS Symp.*, Eur. Space Agency, Mar. 1997.

[13] J. C. Curlander and R. McDonough, *Synthetic Aperture Radar—Systems and Signal Processing.* New York: Wiley, 1991.

[14] G. Schreier, Ed., *SAR Geocoding: Data and Systems.* Karlsruhe, Germany: Wichmann, 1993.

[15] H. Johnsen, L. Lauknes, and T. Guneriussen, "Geocoding of fast delivery ERS-1 SAR image mode product using DEM data," *Int. J. Remote Sensing*, vol. 16, pp. 1957–1968, Nov. 1995.

[16] J. M. Kellndorfer, M. C. Dobson, and F. T. Ulaby, "Geocoding for classification of ERS/JERS SAR composites," in *Proc. IEEE Int. Geosci. Remote Sensing Symp. (IGARSS'96)*, Lincoln, NE, pp. 2335–2337.

[17] L. E. Pierce, J. M. Kellndorfer, F. T. Ulaby, and L. Norikane, "Practical SAR orthorectification," in *Proc. IEEE Int. Geosci. Remote Sensing Symp. (IGARSS'96)*, Lincoln, NE, pp. 2329–2331.

[18] A. Carrara, "Drainage and divide networks derived from high-fidelity digital terrain models," in *Proc. NATO Adv. Study Inst. Stat. Treatments Estimation Mineral Energy Resourc., II Ciocco (Lucca).* Dordrecht, The Netherlands: Reidel, 1986, pp. 581–597.

[19] A. Freeman and J. C. Curlander, "Radiometric correction and calibration of SAR images," *Photogramm. Eng. Remote Sensing*, vol. 55, no. 9, pp. 1295–1301, 1989.

[20] A. Freeman, "SAR calibration: An overview," *IEEE Trans. Geosci. Remote Sensing*, vol. 30, pp. 1107–1121, Nov. 1992.

[21] H. Laur, P. Meadows, J. I. Sanchez, and E. Dwyer, "ERS-1 SAR radiometric calibration," in *Proc. CEOS SAR Calibration Workshop.* Nordwijk, The Netherlands: Eur. Space Agency, ESA WPP-048, 1993, pp. 257–281.

[22] M. Shimada, "User's guide to NASDA's SAR products," Earth Observ. Center, NASDA, HE93014, Mar. 1993.

[23] H. Laur, P. Bally, P. Meadows, J. Sanchez, B. Schättler, and E. Lopinto, *Derivation of the Backscattering Coefficient σ° in ESA ERS SAR PRI Products*, Eur. Space Agency, ES-TN-RS-PM-HL09, issue 2, revision 2, 1996.

[24] M. Shimada, "Radiometric and geometric calibration of JERS-1 SAR," *Adv. Space Res.*, vol. 17, no. 1, pp. 79–88, 1995.

[25] W. Hagg and M. Sties, "Efficient speckle filtering of SAR images," in *Proc. IEEE Int. Geosci. Remote Sensing Symp. (IGARSS'94)*, Pasadena, CA, pp. 2140–2142.

[26] E. S. Kasischke, J. M. Melack, and M. C. Dobson, "The use of imaging radars for ecological applications—A review," *Remote Sens. Environ.*, vol. 59, pp. 141–156, 1997.

[27] T. R. Loveland, J. W. Merchant, D. O. Ohlen, and J. F. Brown, "Development of a land-cover characteristics database for the conterminous U.S.," *Photogramm. Eng. Remote Sensing*, vol. 57, pp. 1453–1463, 1991.

[28] T. R. Loveland, D. O. Ohlen, J. F. Brown, B. C. Reed, Z. Zhu, J. W. Merchant, and L. Yang, "Western hemisphere land cover: Progress toward a global land cover characteristics database," in *Proc. Pecora 13*, U.S. Geol. Survey, 1997.

[29] J. T. Tou and R. C. Gonzalez, *Pattern Recognition Principles.* Reading, MA: Addison-Wesley, 1974.

[30] J. F. Brown, T. R. Loveland, J. W. Merchant, B. C. Reed, and D. O. Ohlen, "Using multisource data in global land cover characteriza-

tion: Concepts, requirements and methods," *Photogramm. Eng. Remote Sensing*, vol. 59, pp. 977–987, 1993.
[31] J. M. Kellndorfer, H. Xie, F. T. Ulaby, and M. C. Dobson, "Combined multi-temporal ERS-1/JERS-1 imagery for land-cover classification," in *Proc. IEEE Int. Geosci. Remote Sensing Symp. (IGARSS'98)*, Seattle, WA.
[32] European Space Agency, *ERS User Handbook.* Noordwijk, The Netherlands: ESA, ESTEC, SP-1148, 1993.

Josef M. Kellndorfer received the diploma degree in physical geography, remote sensing, and computer science, and the Ph.D. degree, both from the University of Munich, Germany, in 1993 and 1998, respectively.

He was a Teaching Assistant at the University of Munich from 1990 to 1993 and held internships at the German Aerospace Research Establishment (DLR) and the German Institute for Applied Geodesy (IfAG). Since 1994, he has been a Visiting Research Scientist at the Radiation Laboratory, The University of Michigan, Ann Arbor. His current research focuses on radar backscatter and SAR image analysis for ecological applications and data integration into geographic information systems (SAR image geocoding and preprocessing techniques). In 1994, he received a doctoral fellowship from the German Academic Exchange Service for research at The University of Michigan.

Leland E. Pierce (S'85–M'85) received B.S. degrees in electrical and aerospace engineering in 1983, and the M.S. and Ph.D. degrees in electrical engineering in 1986 and 1991, respectively, all from The University of Michigan, Ann Arbor.

He has been the Head of the Microwave Image Processing Facility, Radiation Laboratory, Electrical Engineering and Computer Science Department, The University of Michigan, since 1991, where he is responsible for research into the uses of polarimetric SAR systems for remote-sensing applications, specifically, forest canopy parameter inversion.

M. Craig Dobson (M'80–SM'91) received B.A. degrees in geology and anthropology from the University of Pennsylvania, Philadelphia, in 1973 and the M.A. degree in geography from The University of Kansas, Lawrence, in 1981.

He was with the Remote Sensing Laboratory, The University of Kansas Center for Research, Inc., from 1975 to 1984, where he managed several experimental programs related to microwave remote sensing of terrain. He is currently an Associate Research Scientist, The University of Michigan, Ann Arbor. Specific research projects focus on the microwave dielectric properties of soils, microwave sensor response to soil moisture and crop canopy cover using truck-mounted and airborne scatterometers and radiometers, and multitemporal simulations of orbital SAR imagery. Since 1984, he has been with the Radiation Laboratory, The University of Michigan, where he conducts research on the microwave dielectric properties of vegetation and radar backscattering properties of forests.

Fawwaz T. Ulaby (M'68–SM'74–F'80), for a photograph and biography, see p. 879 of the May 1998 issue of this TRANSACTIONS.